Heliyon 10 (2024) e33601

Contents lists available at ScienceDirect

Heliyon

journal homepage: www.cell.com/heliyon

Review article

Lysophosphatidylcholine trigger myocardial injury in diabetic cardiomyopathy via the TLR4/ZNF480/AP-1/NF-kB pathway

Nannan Liu [a,1], Yang Chen [b,1], Tian An [a], Siyu Tao [a], Bohan Lv [a], Jinfang Dou [a], Ruxue Deng [a], Xianjie Zhen [a], Yuelin Zhang [a], Caizhong Lu [c], Zhongsheng Chang [c,**], Guangjian Jiang [a,*]

[a] Traditional Chinese Medicine School, Beijing University of Chinese Medicine, Beijing, China
[b] College of Traditional Chinese Medicine, Xinjiang Medical University, City Urumqi, China
[c] Guangming Traditional Chinese Medecine Hospital of Pudong New Area, Shanghai, China

ARTICLE INFO

Keywords:
Diabetic cardiomyopathy
Lysophospholipids
Lipid metabolism
Gut microbiota
TLR4
ZNF480

ABSTRACT

Background: Diabetic cardiomyopathy (DC), a frequent complication of type 2 diabetes mellitus (T2DM), is mainly associated with severe adverse outcomes. Previous research has highlighted the role of Lysophosphatidylcholine (LPC) in inducing myocardial injury; however, the specific mechanisms through which LPC mediate such injury in DC remain elusive. The existing knowledge gap underscores the need for additional clarification. Consequently, this study aimed to explore the impact and underlying mechanisms of LPC on myocardial injury in DC.

Methods: A total of 55 patients diagnosed with T2DM and 62 healthy controls were involved. A combination of 16s rRNA sequencing, metabolomic analysis, transcriptomic RNA-sequencing (RNA-seq), and whole exome sequencing (WES) was performed on fecal and peripheral blood samples collected from the participants. Following this, correlation analysis was carried out, and the results were further validated through the mouse model of T2DM.

Results: Four LPC variants distinguishing T2DM patients from healthy controls were identified, all of which were upregulated in T2DM patients. Specifically, Lysopc (16:0, 2 N isoform) and LPC (16:0) exhibited a positive correlation with nuclear factor kappa B subunit 2 (*NFKB2*) and a negative correlation with Zinc finger protein 480 (*ZNF480*) Furthermore, the expression levels of Toll-like receptor 4 (TLR4), *c-Jun*, *c-Fos*, and *NFKB2* were upregulated in the peripheral blood of T2DM patients and in the myocardial tissue of T2DM mice, whereas *ZNF480* expression level was downregulated. Lastly, myocardial injury was identified in T2DM mice.

Conclusions: The results indicated that LPC could induce myocardial injury in DC through the TLR4/ZNF480/AP-1/NF-kB pathway, providing a precise target for the clinical diagnosis and treatment of DC.

* Corresponding author. School of Traditional Chinese Medicine, Beijing University of Chinese Medicine Address: No. 11, Bei San Huan Dong Lu, Chaoyang District, Beijing, 100029, China.
** Corresponding author. No. 43 Dongmen Street, Huinan Town, Pudong New Area, Shanghai, China.
E-mail addresses: czs715@163.com (Z. Chang), bucmjiang@163.com (G. Jiang).
[1] Nannan Liu and Yang Chen are the first author.

https://doi.org/10.1016/j.heliyon.2024.e33601
Received 17 August 2023; Received in revised form 15 June 2024; Accepted 24 June 2024
Available online 25 June 2024

Full name	Abbreviation
Lysophosphatidylcholine	LPC/Lysopc
Diabetic cardiomyopathy	DC
Type 2 diabetes mellitus	T2DM
RNA-sequencing	RNA-seq
Whole exome sequencing	WES
Nuclear factor kappa B subunit 2	NFKB2
Zinc finger protein 480	ZNF480
Toll-like receptor 4	TLR4
insulin	INS
liquid chromatography-mass spectrometry	LC-MS/MS
Beijing University of Chinese Medicine	BUCM
fasting plasma glucose	FPG
hemoglobin A1C	HbA1C
traditional Chinese medicine	TCM
creatine kinase-MB	CK-MB
ultra high-performance liquid chromatography-tandem mass spectrometry	UHPLC-MS/MS
Genomic deoxyribonucleic acid	DNA
Polymerase chain reaction	PCR
ethylenediaminetetraacetic acid	EDTA
high-fat diet	HFD
streptozotocin	STZ
hematoxylin and eosin	H&E
Immunohistochemistry	IHC
integrated optical density	IOD
standard deviation	SD
single nucleotide variant	SNV
short-chain fatty acids	SCFAs
Lecithin-Cholesterol Acyltransferase	LCAT
National Center for Biotechnology Information	NCBI
Sequence Read Archive	SRA
Animal Research: Reporting of In Vivo Experiments	ARRIVE

1. Introduction

Diabetic cardiomyopathy (DC) is a prevalent complication of type 2 diabetes mellitus.

(T2DM), which is characterized by cardiac hypertrophy and functional remodeling [1,2]. Epidemiological data revealed that the prevalence of DC in T2DM patients stands at 22 % [3], accounting for 52 % of mortalities in this population [4]. The pathogenesis of DC is multifactorial, involving hyperlipidemia, lipotoxicity, hyperglycemia, and inflammation [5]. Chronic hyperglycemia has been identified as a key risk factor for the onset and progression of DC [6–9]. Nevertheless, the molecular mechanisms underlying lipid metabolism disorder-induced myocardial injury remain elusive. Therefore, understanding the pathogenesis of DC and identifying new molecular targets are crucial for its diagnosis and treatment.

Lysophosphatidylcholine (LPC), essential lipid molecules in mammalian tissues, belong to a category of bioactive lysophospholipids [10]. They play a notable role in glucose-mediated insulin (INS) secretion in diabetic tissues [11]. Prior research has revealed the potential of LPC to induce cardiac muscle atrophy [10,12,13,14,15], although the exact mechanism remains elusive. Hence, the pivotal role of LPC in DC-associated myocardial injury was hypothesized. The gut microbiota's correlation with numerous diseases, including diabetes and cardiovascular disease, has been well-documented, with dysbiosis potentially leading to lipid disorders [16].

LPC have shown to activate *AP*-1 by binding to *TLR4* receptors [10,12]. *ZNF480*, a transcriptional activator of *AP-1*, can regulate cardiac development and function [13]. Furthermore, *AP-1* can interact with *NF-kB* [17,18]. Consequently, in the present study, the TLR4/ZNF480/AP-1/NF-kB pathway was proposed as a key mechanism by which LPC could induce myocardial injury in DC. To probe the effects and mechanisms of LPC on myocardial injury in DC, a multi-omics approach was employed, involving untargeted liquid chromatography-mass spectrometry (LC-MS/MS), 16S rRNA gene amplification sequencing, RNA sequencing (RNA-seq), and whole exome sequencing (WES).

2. Materials and methods

2.1. Human subjects

All study subjects provided the written informed consent and the Ethics Committee of Beijing University of Chinese Medicine (BUCM; Beijing, China; Approval No. 2017BZHYLL0105) approved all the study protocols. This study enrolled 55 patients with T2DM and 62 healthy controls who were admitted to Hepingli Hospital (Beijing, China) between December 2018 and September 2021. Additionally, according to the "Guidelines for Clinical Research on New Chinese Medicines for the Treatment of Diabetes" published by the Ministry of Health of China in 2002 [19], patients with T2DM were concurrently evaluated by three clinical associate chief and

director physicians, who assessed clinical symptoms, conducted tongue examinations, and evaluated pulse characteristics. In the context of traditional Chinese medicine (TCM), the tongue is regarded as a reflection of internal organ health, and its examination may provide valuable insights into the patient's overall systemic health. For millennia, TCM has employed this practice, attributing significance to specific changes in the tongue's appearance, including variations in color, moisture, texture, and the presence of fissures, as potential indicators of cardiovascular disturbances. Inclusion and exclusion criteria are detailed in Table 1. Venous blood and human stool samples were previously collected from consenting human donors, including healthy controls and patients with T2DM. The peripheral venous blood and stool samples were stored at −80 °C until subsequent analysis.

2.1.1. Untargeted LC-MS/MS analysis of human stool samples

In this study, fecal samples (5–10 g) were collected from subjects in the morning and processed for metabolomics analysis using state-of-the-art techniques. Briefly, samples were homogenized in liquid nitrogen and resuspended in 80 % methanol. After centrifugation and dilution, the resulting supernatant was subjected to ultra high-performance liquid chromatography-tandem mass spectrometry (UHPLC-MS/MS) using a Vanquish UHPLC system coupled with an Orbitrap Q ExactiveTMHF mass spectrometer. Raw data files were subjected to sophisticated analytical processing employing Compound Discoverer 3.1 software, which facilitated the precise alignment of chromatographic peaks, the discernment of discrete peaks, and the quantification of metabolites. Subsequently, the structural elucidation of metabolites was achieved by integrating information retrieved from reputable biochemical databases, specifically the Kyoto Encyclopedia of Genes and Genomes (KEGG) (https://www.genome.jp/kegg/pathway.html), the Human Metabolome Database (HMDB) (https://hmdb.ca/metabolites), and the LIPIDMaps (http://www.lipidmaps.org/).

2.1.2. 16S rRNA gene amplicon sequencing of human stool samples

Genomic deoxyribonucleic acid (DNA) extraction was carried out using the cetyltrimethylammonium bromide (CTAB) method, with subsequent evaluation of DNA concentration and purity on 1 % agarose gel. Following adjustment to a concentration of 1 ng/μL using sterile water, specific subregions of the 16S rRNA genes were targeted for amplification employing primers, such as 16S V4: 515F806R, equipped with barcodes. Amplification of the target genomic sequence was achieved through the polymerase chain reaction (PCR) protocol, utilizing a 15 μL aliquot of Phusion® High-Fidelity PCR Master Mix (New England Biolabs, Ipswich, MA, USA). The reaction was primed with 2 μM concentrations of both forward and reverse primers, and commenced with a template DNA quantity of approximately 10 ng. The thermal cycling protocol included an initial denaturation step at 98 °C for 1 min, followed by 30 cycles of denaturation at 98 °C for 10 s, annealing at 50 °C for 30 s, and elongation at 72 °C for 30 s. A final elongation step was conducted at 72 °C for 5 min.The various PCR products were combined in equal-density ratios, and the resulting mixture was visualized by electrophoresis on a 2 % agarose gel. Subsequently, the gel-purified agarose band containing the pooled PCR products was processed using a Qiagen gel extraction kit (Qiagen, Hilden, Germany). Construction of the library was performed in accordance with the manufacturer's recommended protocols, as outlined in the TruSeq® DNA PCR-free Sample Preparation Kit (Illumina, San Diego, CA, USA). This involved the addition of index codes for multiplexed sequencing. The final library underwent sequencing on an Illumina NovaSeq platform, generating 250-bp paired-end reads.

2.1.3. RNA-seq of human peripheral blood samples

Furthermore, venous blood samples, ranging in volume from 8 to 10 mL, were obtained from each participant and subsequently transferred into tubes containing ethylenediaminetetraacetic acid (EDTA) as an anticoagulant. Blood samples were lightly shaken to achieve adequate contact with EDTA, mixed and stored in liquid nitrogen, and then transferred to Novegene laboratory for RNA-seq.

RNA samples were verified using the RNA Nano 6000 assay kit on the Bioanalyzer 2100 system (Agilent Technologies, Santa Clara, CA, USA). In the preparation of RNA samples, a quantity of 1 μg of total RNA was isolated from each individual sample. Sequencing libraries were generated using the NEBNext® Ultra™ RNA library prep kit for Illumina® (NEB, Ipswich, MA, USA) following the manufacturer's protocol, with specific index codes added to link sequences to their respective samples. The generation of clusters for indexed samples was conducted utilizing the cBot Cluster Generation System, employing the TruSeq PE Cluster Kit v3-cBot-HS (Illumina, San Diego, CA, USA), in strict adherence to the protocol outlined by the manufacturer. Subsequently, the library preparations underwent sequencing on an Illumina NovaSeq platform, generating 150-bp paired-end reads.

Table 1
Inclusion and exclusion criteria for T2DM patients and healthy controls.

Criteria Type	T2DM Patients	Healthy Controls
Inclusion	1. Fasting plasma glucose (FPG) level ≥7.0 mmol/L 2. Hemoglobin A1C (HbA1C) level ≥6.5 % 3. Assessment by three clinical associate chief and director physicians considering clinical symptoms, tongue examination, and pulse assessment (TCM)	1. No medical history of metabolic diseases 2. Normal vital signs 3. FPG, HbA1c, and creatine kinase-MB (CK-MB) levels within normal ranges
Exclusion	1. Receipt of antibiotics in the preceding 3 days 2. Pregnancy 3. Chronic illness (heart failure, pulmonary disease, renal failure, gastrointestinal disorders)	1. Receipt of antibiotics in the preceding 3 days 2. Pregnancy 3. Chronic illness (heart failure, pulmonary disease, renal failure, gastrointestinal disorders)

2.1.4. Whole exome sequencing (WES) of human peripheral blood samples

Early morning fasting venous blood of 8–10 mL was collected from patients within 24 h of admission or enrollment and divided into 3 EDTA anticoagulation tubes (2 of which were added at a ratio of 1:3). EDTA anticoagulation tubes (each tube contained at least 3 mL of blood) were utilized for DNA extraction. All blood samples were gently inverted and mixed, and then immediately frozen in liquid nitrogen for subsequent sequencing.

DNA was sheared by sonication, platform-specific adaptors were ligated, and the resulting fragments were size selected. The library was captured using the Agilent Sure Select Human AllExon V6 kit (Agilent Technologies, Santa Clara, CA, USA), and 2 x 75 bp paired-end reads were generated on Illumina PE150 platform (Illumina, San Diego, CA, USA). Reads that did not pass Illumina's standard filters were removed prior to alignment. Remaining reads were aligned to the 1000 Genomes Project (https://www.1000genomes.org/), ESP6500 (http://evs. gs. washi ngton. edu/EVS/), and genome-wide association meta-database (https://gnomad.broadinstitute.org/). Annovar was used for functional annotation of detected variants. Quality filtering was applied by excluding variants found in less than 5 reads and variants detected in less than 15 % variant reads.Variants occurring with a frequency of <1 % were excluded. All remaining calls were checked for correct calling using Integrative Genomics Viewer (IGV, Broad Institute, Cambridge, MA, USA). WES was performed by Novogene Inc. (https://en.novogene.com; Beijing, China).

2.2. Experimental animals

All animal feeding and experiments were approved by the Ethics Committee of the BUCM. In this study, age-matched mice were used. C57bl/6j SPF mice were purchased from Beijing Vital River Laboratory Animal Technology Co., Ltd. (Beijing, China). All mice aged 4-6-week-old at the time of utilization. Mice were housed under controlled conditions at 20–24 °C, with a 12-h light-dark cycle, humidity maintained at 35 % $\pm$ 5 %, and provided with ad libitum access to tap water, all within specific pathogen-free conditions at the BUCM. Besides, the mice were fed with a regular rodent diet (Cat#1022, Beijing Huafukang Biotechnology, Beijing, China).

The total number of mice was 16, of which 8 mice were fed with a high-fat diet (HFD) (Cat#H10045, 45 kcal% fat, Beijing Huafukang Biotechnology) for 8 weeks to induce insulin resistance(recognized as the model group (M)), and 8 mice were fed with a regular rodent diet (Cat#1022, Beijing Huafukang Biotechnology)as the control group (N). Subsequently, both groups of mice were fasted for 12 h. Thereafter, mice in the model group were injected intraperitoneally with freshly prepared streptozotocin (STZ) (in 0.1 M citrate buffer, pH 4.5) once within 24 h to induce a mild increase in insulin secretion and hyperglycemia, while mice in the control group were injected intraperitoneally with an equal amount of saline. After 7 days of injection, fasting blood glucose was examined in both groups by tail vein blood collection, and mice with 6-h FPG $>$11.1 mmol/L were defined as diabetic mice. The glucose was measured every 2 weeks during the experiment.

2.2.1. Histological assessment

Following the procedures of tissue embedding, subsequent sectioning, and the removal of paraffin through the dewaxing process, liver, cardiac, and pancreatic tissues were subjected to histochemical staining employing the Hematoxylin and Eosin (H&E) stain, which facilitates the morphological examination. Furthermore, microscopic examination was conducted to assess the pathology of the liver, heart, and pancreas tissues (magnification, x20).

2.2.2. Immunohistochemistry (IHC)

Tissue samples from the liver, heart, pancreas, and pancreas were fixed using a 10 % neutral-buffered formalin solution (Beijing Yili Fine Chemical Co., Ltd., Beijing, China). Following this, the tissues were embedded in paraffin wax, cooled to increase firmness, and sectioned into 4–5 μm thick slices with a rotary microtome for histological analysis. The slices were dewaxed using adhesive sheets and subsequently baked in an oven at 60 °C. Afterward, the experimental procedures for IHC included antigen retrieval, goat serum blocking, and the application of rabbit anti-TLR4 (1:100; ABclonal, Woburn, MA, USA) and rabbit anti-NFκB2 (1:100; Proteintech). The corresponding secondary antibodies were thereafter utilized for the immunohistochemical detection of TLR4 and NF-κB2. The expression levels of the corresponding antibodies in the tissues were examined under a microscope (magnification, x20) after the detection and blocking of the slices utilizing a laboratory microscope (U-LH100-3; Olympus, Tokyo, Japan). Mean integrated optical density (IOD) values of the positive reactions in each tissue were obtained using Image J software and used for statistical analysis.

2.2.3. Western blotting

Heart tissue was homogenized on ice with five times the volume of RIPA lysate and allowed to stand for 30 min. Following this, centrifugation at 4 °C for 5 min at 12,000 rpm was conducted to remove the supernatant, which was then stored in a −20 °C refrigerator. Subsequently, protein quantification was performed using the BCA kit. The sample was then mixed with 5X protein loading buffer, boiled for 5 min, and promptly stored in an ice bath. The membrane was transferred for 2 h, followed by sealing in 5 % skimmed milk for 1.5 h on a shaker at room temperature. Subsequently, the membrane was thrice washed with 1 $\times$ TBST for 10 min each time. The primary antibodies, such as rabbit anti-TLR4 (1:1000; ABclonal), and rabbit anti-NFκB2 (p100/p52) (1:600; Proteintech) were incubated overnight at 4 °C, followed by thrice rinsing with 1 $\times$ TBST for 10 min each time. The secondary antibody was incubated for 90 min on a shaker at room temperature, and the membrane was thrice washed with 1 $\times$ TBST for 10 min each time. Finally, the ECL solution was prepared, and the membrane was incubated, developed, exposed, and the bands were saved for grayscale analysis using ImageJ software.

2.2.4. RNA extraction and quantitative reverse transcription PCR (qRT-PCR)

Total mRNA was extracted from the peripheral blood of patients and the heart tissues of mice using TRIzol total RNA isolation reagent. Thereafter, cDNA was prepared using the cDNA synthesis kit (Novoprotein Scientific Inc, Suzhou, China). The cDNA input was standardized to β-actin. Subsequently, quantitative real-time polymerase chain reaction (qRT-PCR) was conducted in a total volume of 20 μL using the Applied Biosystems 7500 system. All samples were pre-incubated at 95 °C for 10 min and then subjected to 42 amplification cycles (95 °C for 20s, 60 °C for 60 s). The annealing temperature of all primers was 60 °C. Relative gene expression was calculated using the $2^{-\triangle\triangle CT}$method. The primers used for the qRT-PCR experiment are listed in Table 2.

2.3. Statistical analysis

Statistical analyses were conducted to determine differences between groups. The Student's t-test (two-tailed) was applied to datasets that demonstrated a Gaussian distribution. In cases where datasets deviated from a normal distribution and exhibited nonparametric properties, the Kruskal-Wallis H test was utilized. The results of these analyses were then presented, with each dataset reported as the mean ± standard deviation (SD). Statistical tests used to compare conditions are specified in figure legends (*$q < 0.05$, *$q < 0.01$; *$p < 0.05$, **$p < 0.01$), with $q < 0.05$ and $p < 0.05$ considered statistically significant. Moreover, R (R version R-3.4.3, R 4.1.0), SPSS software (version 26.0; IBM, Armonk, NY, USA), and GraphPad Prism (GraphPad Software Inc., San Diego, CA, USA) software were used for the generation of graphs and performing statistical analysis.

3. Results

3.1. Baseline clinical characteristics of the subjects

A total of 117 subjects were enrolled in this study, including 62 healthy controls as the N group and 55 patients with T2DM as the T2DM group. To indicate whether the enrolled subjects have T2DM, biochemical tests were conducted on the peripheral blood samples. The results revealed that all T2DM patients met the diagnostic criteria for T2DM. There were significant increases in the levels of FPG, HbA1c, and CK-MB between the T2DM group and the N group ($p < 0.05$). No significant difference in age was found between the two groups (Table 3).

3.2. Gut microbiome in incident cases of T2DM

To explore the alterations and functional implications of specific intestinal microbiota in T2DM, we performed 16S rRNA gene amplicon sequencing was performed on all participants enrolled in this study. It was found that compared with the N group, T2DM patients had dysbiosis, with a significant decrease in the abundance of *Romboutsia* and *Roseburia* ($p < 0.01$) (Fig. 1A).

Additionally, functional prediction of the different gut flora in the N and T2DM groups was performed using the TaxFun algorithm. It was revealed that the function was mainly related to lipid metabolism ($p < 0.05$), the immune system ($p < 0.001$) and cardiovascular disease ($p < 0.001$) (Fig. 1B).

We further conducted a correlation analysis to assess the association between these distinct intestinal microbiotas and clinical indicators such as FPG, HbA1C, and CK-MB levels in the T2DM and N groups.The results indicated that *Romboutsia*, *Roseburia*, *Turicibacter*, *Faecalibacterium* and *Anaerostipes* were negatively correlated with FPG and CK-MB levels. *Bifidobacterium* and *Lactobacillus* were positively correlated with FPG level ($p < 0.05$)(Fig. 1C).

3.3. LPC in incident cases of T2DM

To evaluate the differences in concentrations of LPC, fecal specimens were obtained from all study participants, and an untargeted

Table 2
mRNA primers for qRT-PCR analysis.

Primer name	Sequence
ZNF480	F:5′ GTCAGGGATGGCTCTTCCTCAGG 3′ R:5′ AGGGTCCAGGCATTTCCACTCC 3′
c-Jun	F:5′-TGGGCACATCACCACTACAC-3′ R: 5′-TCTGGCTATGCAGTTCAGCC-3′
c-Fos	F:5′-CAACACACAGGACTTTTGCG-3′ R:5′-GGAGATAGCTGCTCTACTTTG-3′
TLR4	F:5′-AGAAATTCCTGCAGTGGGTCA-3′ R:5′-TCTCTACAGGTGTTGCACATGTCA-3′
Cd36	F: 5′-CAGGCTTTGTTGGGACAGAC-3′ R: 5′-GCTAATTTGTGGTTGGTTGCCA-3′
NFKB2	F: 5′-TTCTCCTAGACCTCTGCCCG-3′ R: 5′-AGCAGCTTAGGAAAGTCCCG-3′
β-actin	F: 5′-GTGGCCGAGGACTTTGATTG-3′ R: 5′-CCTGTAACAACGCATCTCATATT-3′

Table 3
Baseline clinical characteristics of the subjects.

	N	T2DM	P value
Number	62	55	–
Male/female	30/32	30/25	–
Age	54.52 ± 11.19	56.98 ± 8.81	0.207
FPG	5.51 ± 0.95	10.60 ± 4.08	< 0.001
HbA1c	5.65 ± 0.34	8.58 ± 2.01	< 0.001
CK-MB	6.50 ± 2.38	10.24 ± 3.46	0.046

LC-MS/MS assay was employed. The results revealed that there were four LPC variants in the T2DM group compared with the N group, and their concentrations were elevated in the T2DM group, including a 2.32-fold increase in LPC 16:0, a 2.09-fold increase in Lysopc 16:0 (2 N Isomer) and a 1.55-fold increase in LPC 17:0 ($p < 0.01$) (Table 4).

To further explore the potential associations, correlation analysis was conducted involving LPC, significantly altered gut microbiota, and levels of FPG, HbA1C, and CK-MB. The findings indicated that LPC (16:0), Lysopc (16:0, 2 N Isomer), and LPC (17:0) were positively correlated with both FPG and CK-MB levels (Fig. 2A). Additionally, LPC (16:0), Lysopc (16:0, 2 N Isomer), and LPC (17:0) exhibited negative correlations with *Romboutsia, Roseburia, Turicibacter*, and *Faecalibacterium* ($p < 0.05$) (Fig. 2B), while displaying positive correlations with *Bifidobacterium* and *Lactobacillus*.

3.4. Peripheral blood RNA-seq findings in T2DM patients

To elucidate the pathogenic mechanisms by which LPC induce DC, RNA-seq was performed on peripheral blood samples from the subjects and conducted a correlation analysis was conducted to identify associations between LPC levels and differentially expressed mRNAs.The results showed that the expression levels of *LCAT*, and *NFKB2* were upregulated by 0.65-fold ($p < 0.05$), and 0.48-fold ($p < 0.01$), respectively, in the T2DM group compared with the N group. In addition, *ZNF480* expression level was downregulated by 0.21-fold in the T2DM group ($p < 0.01$) (Table 5). The *LCAT* gene encodes for the enzyme lecithin-cholesterol acyltransferase, playing a pivotal role in the biosynthesis of LPC. The correlation analysis of LPC and mRNAs indicated that Lysopc (16:0,2 N Isomer) and LPC (16:0) were positively correlated with *NFKB2*, while negatively correlated with *ZNF480* (Fig. 3A).

3.5. The WES results and combined RNA-DNA analysis

To further explore the pathological mechanisms by which LPC contribute to DC, the WES was carried out on the subjects' peripheral blood samples, and screening was conducted to identify mutations shared among 2 or more T2DM patients. It was found that *ZNF480* was mutated in 12 T2DM patients with 3 mutated loci; and *TLR4* was mutated in 2 T2DM patients with 4 mutated loci. Additionally, the analysis has revealed that the gene *ZNF480* gene contained both a frameshift deletion and a stopgain mutation, whereas *TLR4* gene was marked by a frameshift deletion and a missense single nucleotide variant (SNV). These mutations were recognized as substantive modifications with the potential to influence gene expression and modulate protein functionality (Table 6).

Besides, utilizing combined RNA-DNA analysis, it was determined that the *ZNF480* gene included mutations, specifically frameshift deletions and stopgain mutations, in 13 patients diagnosed with T2DM (Table 7). In addition, compared with the N group, *ZNF480* expression level was downregulated by 0.2-fold in the T2DM group ($p < 0.01$), while *NFKB2* expression level was upregulated by 0.48-fold ($p < 0.01$) (Fig. 3B).

Further pathway enrichment analysis of the differentially expressed genes shared at the DNA and RNA levels revealed that the pathways were mainly associated with heart development, Toll-like receptor 4 signalling pathway, and positive regulation of NIK/NF kappaB signalling pathway, and so on (Fig. 3C).

The qRT-PCR was employed to detect the expression levels of *ZNF480*, and *NFKB2* in the subjects' peripheral blood samples, and the results were consistent with those of RNA-seq ($p < 0.05$) (Fig. 3D and E). The expression levels of TLR4, c-Jun, and c-Fos were also examined, in which they were upregulated in the T2DM group compared with the N group ($p < 0.05$) (Fig. 3F–H, I).

3.6. Establishment of a mouse model of T2DM

To further validate the aforementioned experimental results, a mouse model of T2DM was established. The results showed that serum levels of FPG and insulin (INS) were elevated in the model group (M) compared with those in the normal group (N)($p < 0.01$) (Fig. 4A and B).

3.7. Hepatic pathological changes of mice with T2DM

Given the strong correlation between increased LCAT activity and the development of hepatic steatosis, histopathological evaluations of liver tissues from the T2DM murine models was performed to investigate the occurrence of steatosis in the hepatic system. The results indicated that the liver tissue of mice in the N group had intact hepatic lobules, with hepatocytes arranged radially around the central vein and the nuclei centered. Compared with the N group, the liver tissue of the mice in the M group exhibited a discernible

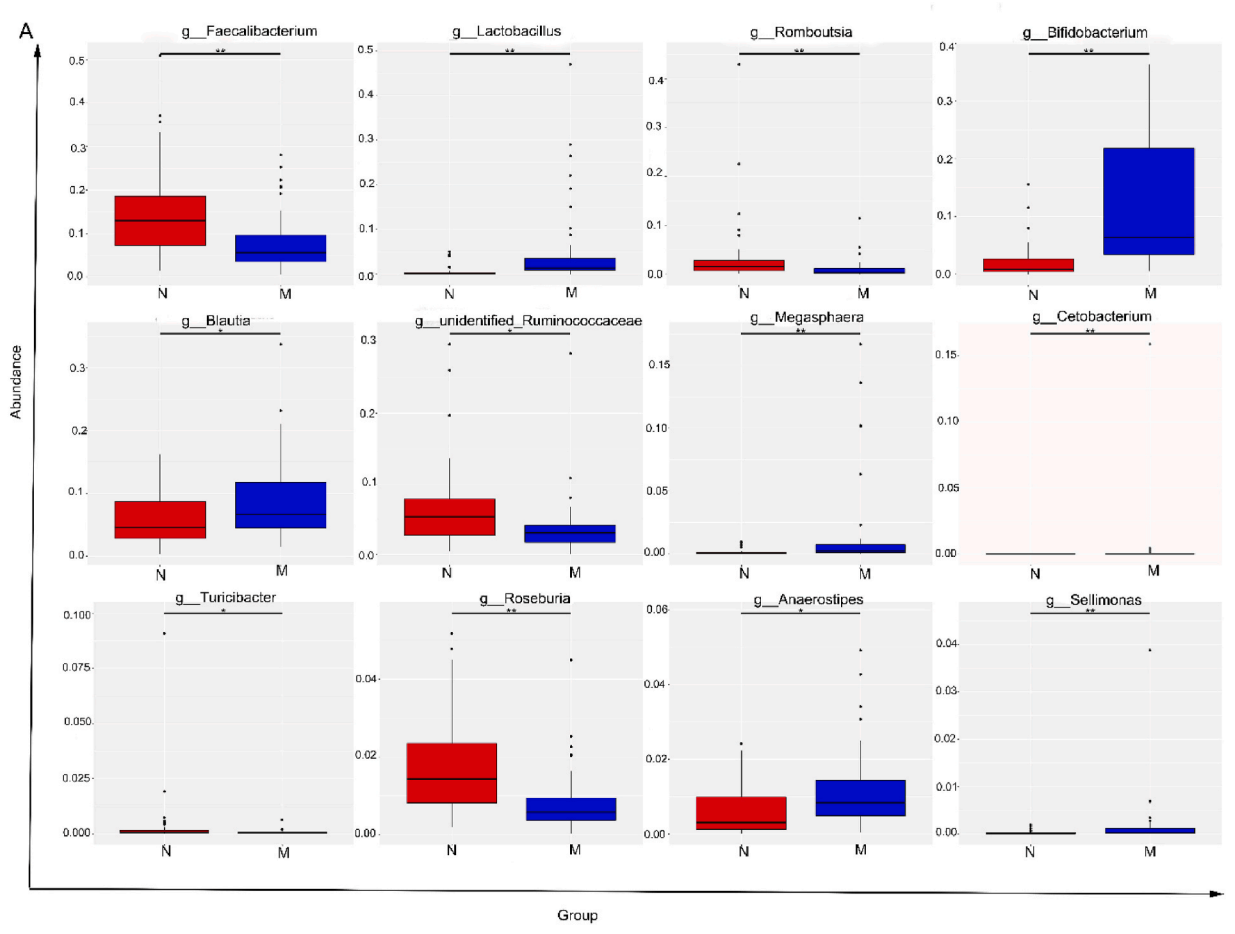

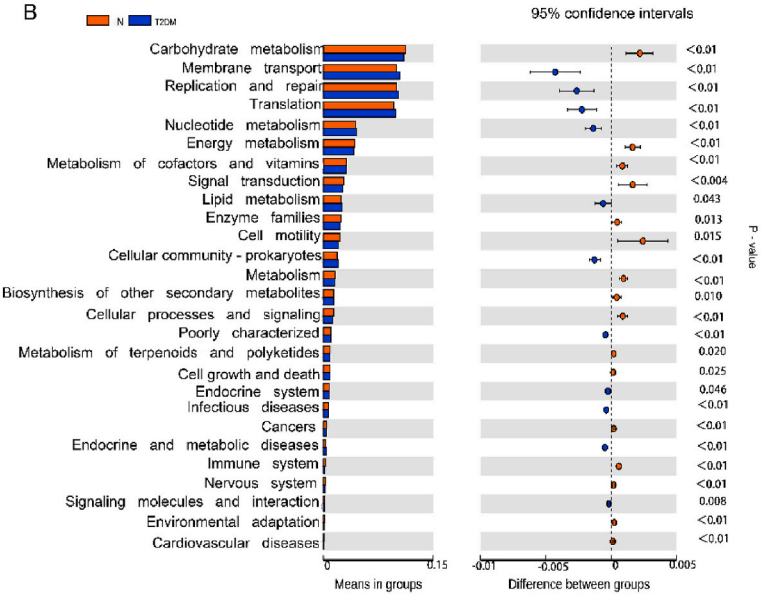

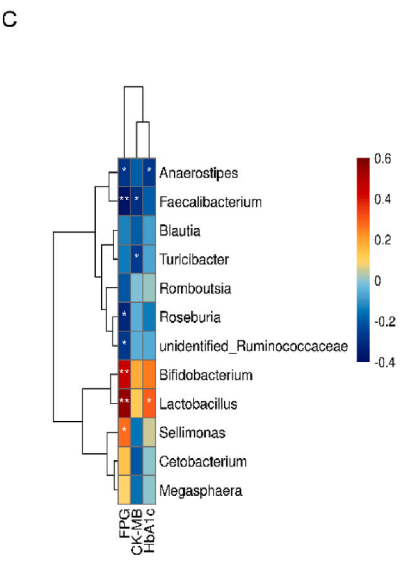

(caption on next page)

Fig. 1. Gut microbiome in T2DM incident and the relationship between gut flora and clinical baseline indicators. (A) Significant differences in gut microbes between T2DM and N groups. *q < 0.05,**q < 0.01 as determined by MetaStat analysis. q < 0.05 was considered significant. (B) Functional prediction of gut microbiota with significant differences between T2DM and N groups. *p < 0.05,**p < 0.01 as determined by Taxfun algorithm. p < 0.05 was considered significant. (C) Association analysis between gut microbiota and baseline clinical characteristics of the subjects. *p < 0.05,**p < 0.01 as determined by spearman analysis. p < 0.05 was considered significant.

Table 4
The lysophosphatidylcholine variants between T2DM and N groups (feces).

Compound_ID	Name	FC	log2FC	P value	Up.Down
Com_6399_neg	LPC 16:0	4.993613938	2.320084289	0.010853785	up
Com_18901_neg	LPC 17:0	2.924371619	1.548126656	0.027200252	up
Com_3988_neg	Lysopc 16:0 (2 N Isomer)	4.250803387	2.087735531	0.001284473	up
Com_11350_neg	Lysopc 15:0	4.443717735	2.151767179	0.0185915	up

LPC 16:0: lysophosphatidylcholine with palmitic acid; LPC 17:0: lysophosphatidylcholine with margaric acid; Lysopc 15:0: lysophosphatidylcholine with pentadecanoic acid; Lysopc 16:0 (2 N Isomer): the 2-N isomer of Lysophosphatidylcholine with a palmitic acid chain.

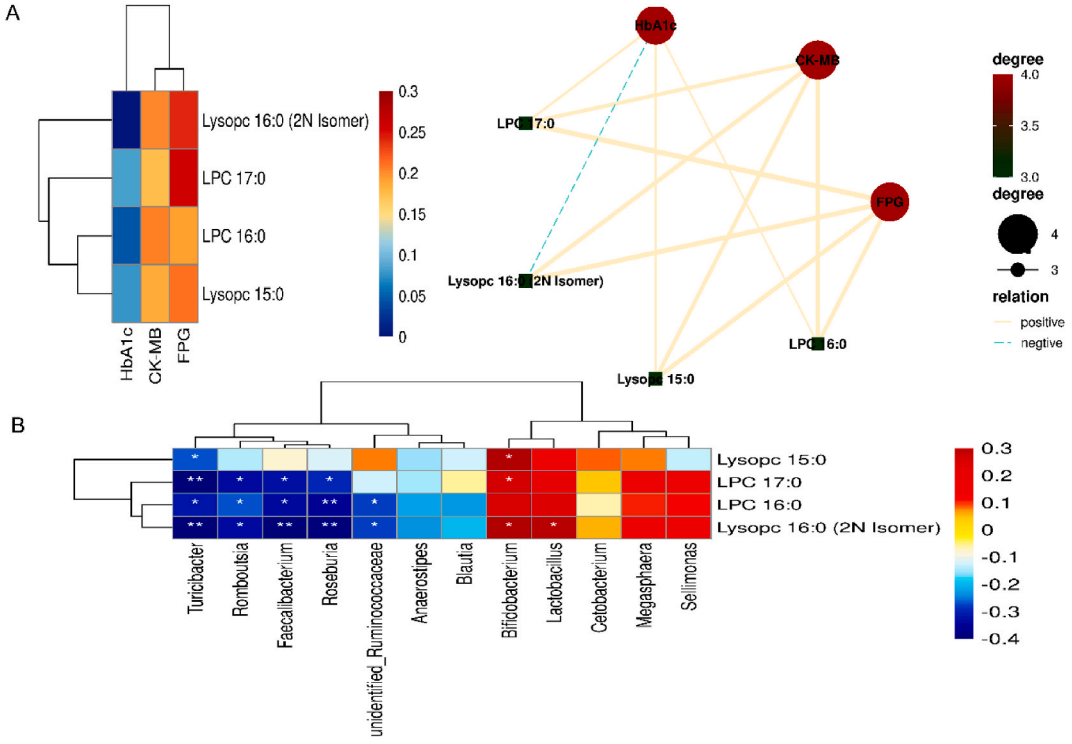

Fig. 2. Association analysis between LPC, gut microbiota, and baseline clinical characteristics of the subjects.(A) The relationship between LPC and baseline clinical characteristics of the subjects.(B) The relationship between LPC and gut microbiota. *p < 0.05,**p < 0.01 as determined by spearman analysis. p < 0.05 was considered significant.

lobular structure, disorganized hepatic cords, fatty vacuole-like changes of varying sizes in the hepatocyte mass, and some nuclei were deviated to one side (Fig. 4C).

3.8. Histopathological examination and assessment of TLR4 expression level in the pancreas of mice with T2DM

For the purpose of validating the establishment of the T2DM murine model and elucidating TLR4 expression level in the pancreas, histological assessments, including H&E staining and IHC were performed on pancreatic tissues from the T2DM mice to provide detailed tissue characterization. The results of H&E staining revealed that the pancreatic islets in the N group had normal size and a regular shape, without congestion, edema, or inflammatory cell infiltration.Compared with the N group, mice in the M group exhibited irregularly shaped pancreatic islets, notable lipid vacuolization, diminished size and quantity of pancreatic islet cells, along with inflammatory cell infiltration, and degeneration necrosis in the pancreatic tissue. (Fig. 4D). Additionally, the expression level of TLR4 was elevated in the pancreatic tissue of mice in the M group compared with that in the N group (Fig. 5A–B).

Table 5
mRNA changes between T2DM and N groups (peripheral blood).

gene_id	gene_name	log2FoldChange	P value	padj
ENSG00000213398	*LCAT*	0.336587339	0.031784194	0.114540784
ENSG00000198464	*ZNF480*	−0.207562922	0.003060756	0.018113872
ENSG00000077150	*NFKB2*	0.478790168	1.51E-09	8.18E-08
ENSG00000135218	*CD36*	0.083062468	0.346438924	0.604480962

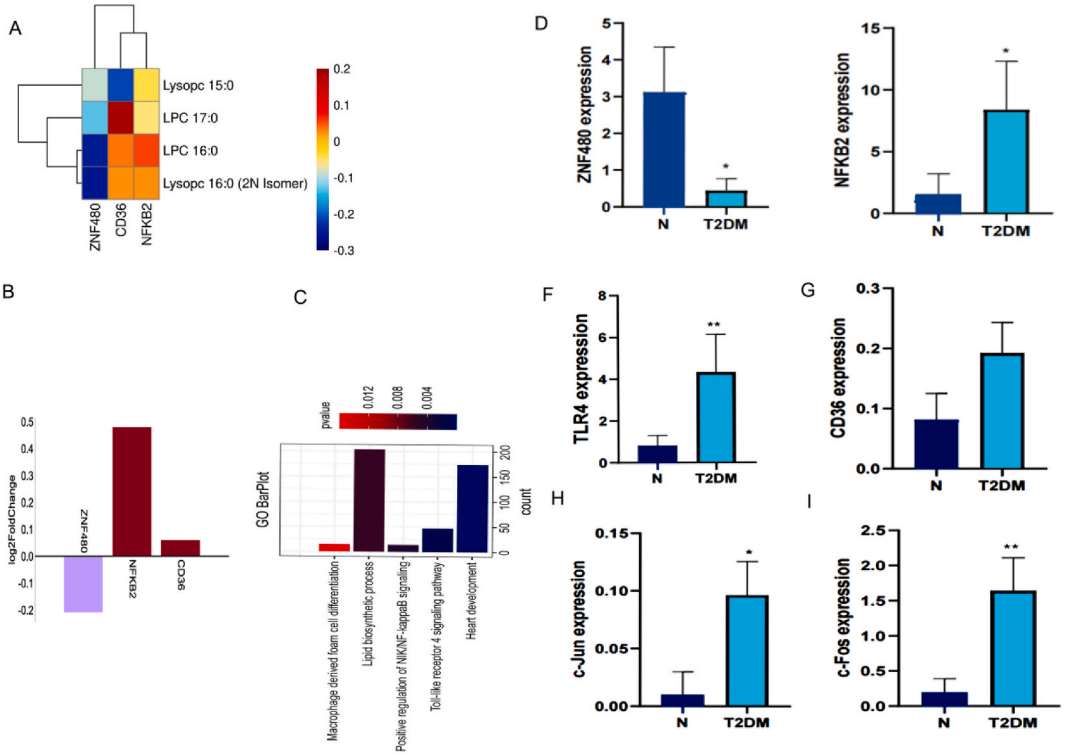

Fig. 3. Association analysis of LPC and mRNAs, and RNA-DNA conjoint. (A) Association analysis between *ZNF480*, *NFKB2*, *CD36,* and LPC. (B) Log2FoldChange of *ZNF480*, *NFKB2*, and *CD36*. *$p < 0.05$,**$p < 0.01$ as determined by spearman analysis. $p < 0.05$ was considered significant. Purple represents down-regulation, and red represents up-regulation. (C) The GO pathway of differentially expressed genes shared at the DNA and RNA levels. Expression of (D) *ZNF480*, (E) *NFKB2*, (F)*TLR4*, (G) *CD36*, (H)*c-Jun*, (I) *c-Fos* in peripheral blood of T2DM patients. *$p < 0.05$, **$p < 0.01$ as determined by two-tailed Student's t-test, and Kruskal-Wallis H. $p < 0.05$ was considered significant.

Table 6
The **WES results of peripheral blood of T2DM patients (peripheral blood).**

Priority	CHROME	POS	ID	REF	ALT	QUAL	GeneName	Mutation	PatientSharedNumber
H	19	52803668	rs760772309	GCT	G	88	*ZNF480*	frameshift deletion	12
H	19	52803673	.	G	GA	137	*ZNF480*	stopgain	12
H	19	52825329	rs367935805	C	T	222	*ZNF480*	stopgain	12
H	7	80290381	rs777437579	T	C	222	*CD36*	missense SNV	5
H	7	80290384	rs70961715	G	C	222	*CD36*	missense SNV	5
H	7	80292448	rs143150225	C	T	222	*CD36*	missense SNV	5
H	7	80292492	rs771055875	A	G	222	*CD36*	.	5
H	7	80293720	rs745604189	A	G	70	*CD36*	.	5
H	7	80293774	rs748431584	TAAGTA	T	222	*CD36*	frameshift deletion	5
H	7	80295807	.	T	C	194	*CD36*	.	5
H	7	80302116	rs148910227	C	T	222	*CD36*	missense SNV	5
H	7	80290381	rs777437579	T	C	222	*CD36*	missense SNV	5
H	9	120474683	rs56302444	A	G	222	*TLR4*	missense SNV	2
H	9	120476348	rs201233099	G	A	222	*TLR4*	missense SNV	2
H	9	120476504	rs758837745	G	GT	222	*TLR4*	frameshift insertion	2
H	9	120476846	rs55751501	G	A	222	*TLR4*	missense SNV	2

Table 7
RNA -DNA conjoint analysis results.

Priority	CHROME	POS	ID	REF	ALT	GeneName	Mutation	PatientSharedNumber
H	19	52803668	rs760772309	GCT	G	*ZNF480*	frameshift deletion	13
H	19	52803673	.	G	GA	*ZNF480*	stopgain	13
H	19	52825329	rs367935805	C	T	*ZNF480*	stopgain	13
H	7	80290381	rs777437579	T	C	*CD36*	missense SNV	2
H	7	80290384	rs70961715	G	C	*CD36*	missense SNV	2
H	7	80292448	rs143150225	C	T	*CD36*	missense SNV	2
H	7	80292492	rs771055875	A	G	*CD36*	.	2
H	7	80293720	rs745604189	A	G	*CD36*	.	2
H	7	80293774	rs748431584	TAAGTA	T	*CD36*	frameshift deletion	2
H	7	80295807	.	T	C	*CD36*	.	2
H	7	80302116	rs148910227	C	T	*CD36*	missense SNV	2
H	7	80302123	rs201355711	A	T	*CD36*	missense SNV	2

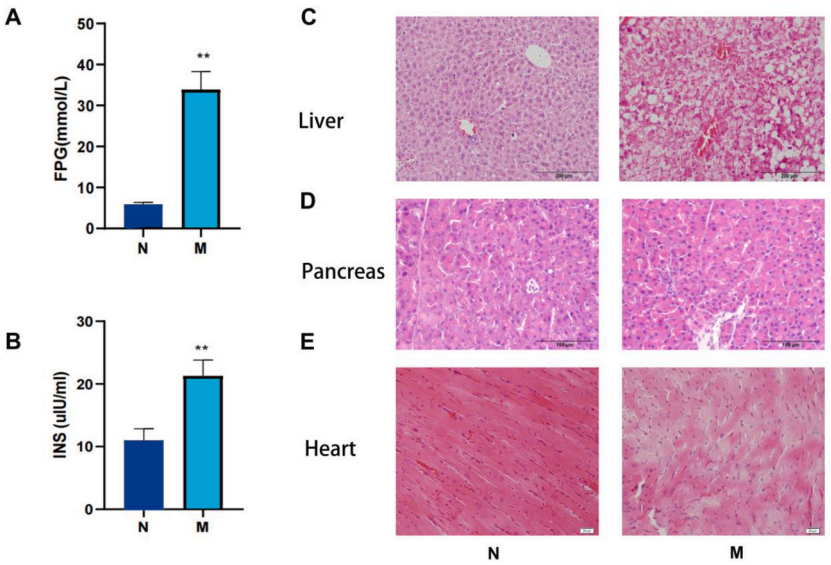

Fig. 4. Changes of blood indexes and H&E staining of liver, pancreas, and heart tissues in N and M groups.The levels of serum (A) FPG, (B) INS of T2DM model mice. $*p < 0.05$,$**p < 0.01$ as determined by two-tailed student's t-test. $p < 0.05$ was considered significant. (C)The H&E staining of the liver, (D) pancreas, and (E) heart tissues. The magnification of the liver tissues is × 20. The magnification of both the pancreas and heart tissues is × 40.

3.9. Histopathological examination and alterations in gene expression in the heart tissues of mice with T2DM

To explore the potential myocardial structural alterations associated with the progression of Type 2 Diabetes Mellitus (T2DM) and the underlying mechanisms mediated by lipopolysaccharide-primed monocytes (LPC) in the pathogenesis of diabetes, we conducted comprehensive histopathological assessments was conducted on myocardial samples from T2DM mice models. These assessments involved H&E staining, Western blotting analysis, and qRT-PCR to precisely evaluate the cardiac tissue at both the morphological and molecular levels.The results of H&E staining results showed that the structure of myocardial tissue of mice in the N group mice was clear, the myocardial cells were arranged neatly, and no inflammatory cell infiltration was found. Compared with the N group, the myocardial tissue in the M group exhibited granular degeneration, involving myocardial cell edema, and steatosis. The nuclear chromatin was blurred, and the myocardial structure was disordered (Fig. 4E).

In addition, the results of Western blotting and qRT-PCR indicated that compared with the N group, the expression levels of TLR4, NFKB2 (Fig. 5C–K),*TLR4*, *c-Jun, c-Fos* and *NFKB2* (Fig. 5M–P) in the heart tissue of mice in the M group mice increased ($p < 0.05$), while the expression level of *ZNF480* decreased ($p < 0.05$) (Fig.5L).

4. Discussion

Notably, T2DM escalates the risk of DC [20], which is a common T2DM-associated complication [8,21]. CK-MB, a recognized myocardial injury biomarker, is considered as a primary clinical indicator for the early diagnosis of DC [3]. Abukhalil et al. reported a significant surge in serum CK-MB level in diabetic rats in a DC model established with intraperitoneal streptozotocin (STZ) injection [7,

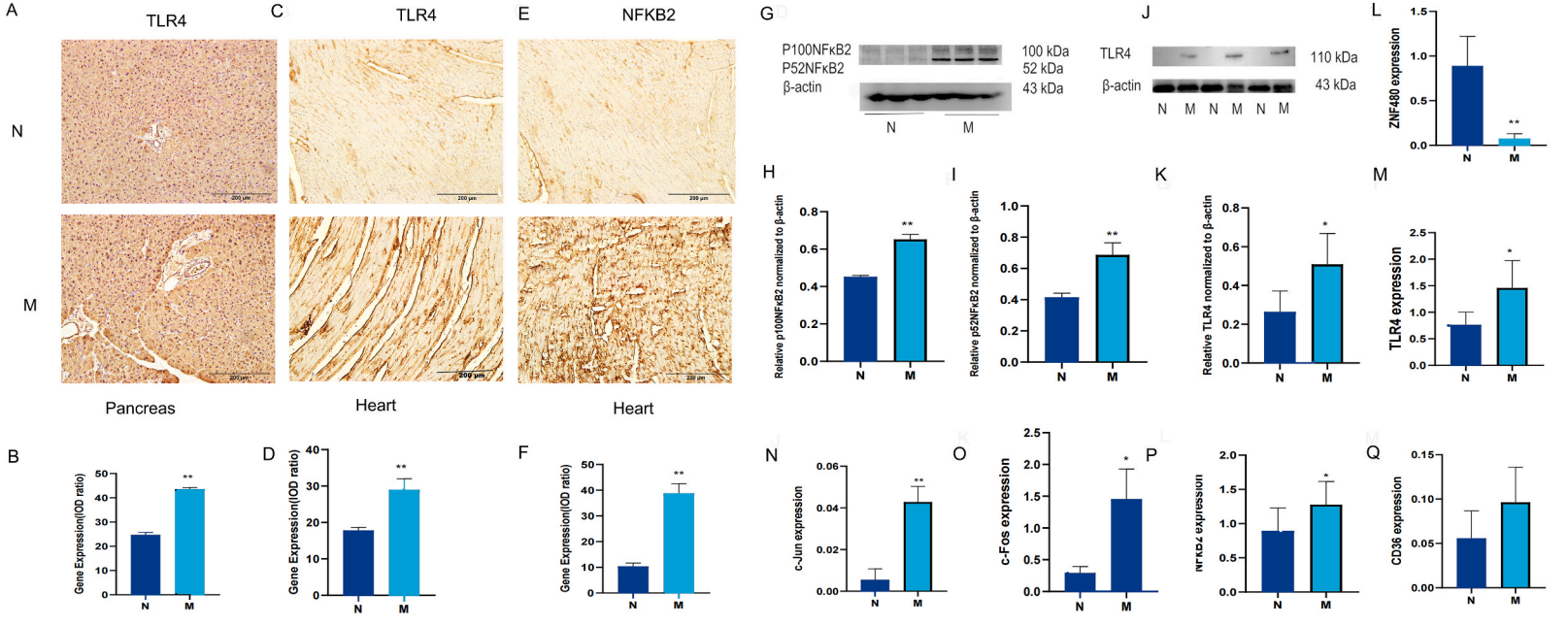

Fig. 5. Gene expression of pancreatic and heart tissues of mice with T2DM. (A) and (B) TLR4 expression of mouse pancreatic tissues between N and M group (magnification was × 20). (C–K) TLR4, and NFKB2 expression of mouse cardiac tissue between N and M group (magnification of images C and E was × 20). (L) *ZNF480*, (M) *TLR4*, (N) *c-Jun*, (O) *c-Fos*, (P) *NFKB2*, and (Q) *CD36* expression of mouse cardiac tissue between N and M group. $*p < 0.05$,$**p < 0.01$ as determined by two-tailed student's t-test. $p < 0.05$ was considered significant.

22]. Elevated serum CK-MB level is deemed indicative of myocardial injury [14]. Consistent with this finding, the elevated serum CK-MB level was found in the T2DM group compared with the N group in the present study. It is evident that all T2DM patients enrolled in this study presented with diabetic cardiomyopathy and myocardial injury.

The present study revealed an association between T2DM patients and dysbiosis, which was characterized by a significant reduction in the abundance of *Romboutsia* and *Roseburia*. This reduction was negatively correlated with FPG level, which exhibited an elevated levels in the T2DM group compared with the N group. Prior research by our team and others demonstrated the increased serum FPG levels in T2DM patients or T2DM mouse models [23–25]. Hyperglycemia is an independent risk factor for DC [6,21]. The resulting hyperglycemia can trigger glucotoxicity, contributing to cardiac injury [26]. Moreover, the role of *Romboutsia* in the regulation of glucose homeostasis regulation through butyrate formation has been previously reported [27]. *Roseburia is also a* butyrate-producing bacterium [28]. Butyrate is recognized as a key mediator in the gut microbiota's regulation of glucose metabolism [29] and it can ameliorate hyperglycemia. Zhang Ling et al. found that butyrate could be protective against cardiac metabolic disorders in T2DM mice [30]. Previous studies have shown a correlation between CK-MB levels and glucose levels [31]. The present study also identified a negative correlation between *Romboutsia* and *Roseburia* with both FPG and CK-MB levels. Hence, it was hypothesized that the reduced abundance of *Romboutsia* and *Roseburia* in the context of T2DM pathology might lead to hyperglycemia by affecting butyrate synthesis, ultimately inducing myocardial injury in DC.

The influences of *Romboutsia* on hepatic lipogenesis and fat accumulation in rats have been documented [29]. Hepatic lipogenesis, responsible for the production of vital lipids for systemic lipid metabolism, is dependent on bacterial-derived short-chain fatty acids (SCFAs) [32]. Butyric acid is an essential regulator of lipid metabolism [28], which is a SCFA produced by the intestinal microbiota [33]. *Romboutsia* is butyric acid -producing bacteria. Zhao et al. found that butyric acid could inhibit hepatic steatosis [34]. Hepatic steatosis constitutes a critical pathophysiological substrate that contributes to the augmented activity of LCAT within the pathological context of T2DM. In the present study, it was revealed that the differential gut flora function in the normal (N) and T2DM groups was primarily related to lipid metabolism, and the liver of T2DM model mice exhibited fatty vacuolar degeneration. Consequently, we posit that the low abundance of *Romboutsia* might affect hepatic lipogenesis via reducing butyrate production, resulting in hepatic steatosis. LCAT (Lecithin-Cholesterol Acyltransferase) is secreted by the liver and circulates in the blood, playing a pivotal role as the key enzyme responsible for the liver's conversion of PC into LPC [22,35]. Evidence has suggested the increased LCAT activity in the blood of patients and rats with hepatic steatosis [36,37], leading to a notable LPC production [38]. In the present study, *LCAT* expression level was found to be upregulated by 0.65-fold in the peripheral blood of T2DM patients. Furthermore, all four differential LPC exhibited increased levels. Among them, LPC (16:0), Lysopc (16:0,2 N Isomer), and LPC (17:0) were negatively correlated with *Romboutsia*. Collectively, we postulate that a lower abundance of *Romboutsia* could lead to the decreased butyric acid production, which could potentially contribute to the development of hepatic steatosis. This condition may, in turn, be a fundamental factor in the enhanced activity of LCAT within the circulatory system, potentially resulting in the elevated levels of LPC. Higher levels of LPC have been demonstrated to induce islet dysfunction [8,9], resulting in insulin resistance, a central pathogenic feature of T2DM [39]. The present indicated the increased levels of LPC in T2DM patients, accompanied by degeneration and necrosis of pancreatic islets, as well as the elevated serum insulin levels in T2DM mice. Thus, it is apparent that the high levels of LPC may trigger T2DM by promoting insulin resistance.

The myocardial injury in T2DM mice was also revealed in the present study. Previous research has demonstrated that the elevated levels of LPC could induce structural damage to the myocardium, potentially initiating and exacerbating DC [40,41]. Additionally, a correlation was identified between LPC and CK-MB [42]. However, the underlying mechanism remains elusive. Consequently, the subjects' peripheral blood samples underwent RNA-seq and WES, and the combined RNA-DNA analysis was conducted to identify the key LPC targets in DC. The findings indicated that *ZNF480* was mutated in 13 patients, accounting for 23.64 % of T2DM patients, and its expression level was downregulated equal to 0.2-fold. Additionally, *TLR4* mutations were identified in two T2DM patients, and *NFKB2* was upregulated by 0.48-fold in T2DM patients.

The key enriched pathways identified by differentially expressed genes at both RNA and DNA levels were the Toll-like receptor 4 signaling pathway and the positive regulation of NIK/NF-kappaB signaling pathway. Consistently, in both human subjects and T2DM mice, the expression levels of *ZNF480* and *NFKB2* followed the RNA-seq outcomes. The expressions levels of *TLR4*, *c-Jun*, and *c-Fos* (the main components of AP-1) were found to be upregulated in T2DM patients and in the myocardial tissue of T2DM mice. Prior studies reported that the upregulation of the expression levels of both *c-Fos* and *c-Jun* could trigger myocardial apoptosis [14,15]. Moreover, LPC could activate the AP-1 signaling pathway through TLR4 binding [10,12,43]. Thus, it is evident that LPC may induce myocardial injury in DC via the TLR4/AP-1 pathway.

ZNF480 is a unique zinc-finger gene, which is predominantly found in the heart. Prior research demonstrated that *ZNF480* could contribute to myocardial fibrosis via the MAPK signaling pathway [13], serving as an upstream signaling protein for *AP-1* [44]. Yi et al. identified *ZNF480* as a transcriptional activator for *AP-1* [13]. Furthermore, *AP-1* can interact with *NF-kB* [17,18]. *NFκB2* is a member of the *NF-κB* family. Westbrook et al. reported that the elevated expression level of *NF-kB* can lead to cardiac muscle weakness [45]. Collectively, we conjecture that LPC may induce myocardial injury in DC via the TLR4/ZNF480/AP-1/NF-kB pathway.

5. Conclusion

In conclusion, by integrating human-level multi-omics analysis with animal-level validation, it was revealed that LPC could trigger myocardial injury in DC via the TLR4/ZNF480/AP-1/NF-kB pathway, thereby emerging as a potential target for the treatment of DC. In addition, the identified limitations, such as the absence of mechanistic insights, will be addressed in the future research endeavors. This will involve studying genetically modified animal models and investigating fecal microbiota transplantation in animal models showing

symptoms of T2DM.

Data availability statement

The sequence data underlying this study are deposited in the National Center for Biotechnology Information (NCBI) Sequence Read Archive (SRA) and can be retrieved using the accession number SRP444531, along with the corresponding project number PRJNA984820.

Funding

This work was supported by National Natural Science Foundation Committee (China. grant number: 82260931, PWR-zm2020-11, PKJ-2021-Y65 and 81460705).

Ethics statement

Human

This study was reviewed and approved by the Ethics Committee of the Beijing University of Chinese Medicine (BUCM), with the approval number: (#2017BZHYLL0105). All protocols adhered to the tenets of the *Declaration of Helsinki*, and both investigators and subjects maintained confidentiality. All participants provided informed consent to participate in the study and to have their anonymised case details published.

Animals

We ensured that the work described has been carried out in accordance with the U.K. Animals (Scientific Procedures) Act, 1986 and associated guidelines. All animal studies complied with the Animal Research: Reporting of In Vivo Experiments (ARRIVE) guidelines. In addition, all animal feeding and experiments were approved by the Ethics Committee of the BUCM (#BUCM-4-2018112701-4049). The study complies with all regulations.

Statements on consent to participate and consent to publish

All participants gave written informed consent and consented to publication.

CRediT authorship contribution statement

Nannan Liu: Writing – review & editing, Writing – original draft. **Yang Chen:** Writing – review & editing. **Tian An:** Methodology, Data curation. **Siyu Tao:** Conceptualization. **Bohan Lv:** Methodology. **Jinfang Dou:** Conceptualization. **Ruxue Deng:** Conceptualization. **Xianjie Zhen:** Conceptualization. **Yuelin Zhang:** Methodology. **Caizhong Lu:** Validation, Conceptualization. **Zhongsheng Chang:** Conceptualization. **Guangjian Jiang:** Conceptualization.

Declaration of competing interest

The authors declare that they have no known competing financial interests or personal relationships that could have appeared to influence the work reported in this paper.

Acknowledgments

We would like to thank Beijing Hepingli Hospital and National Natural Science Foundation Committee.

Appendix A. Supplementary data

Supplementary data to this article can be found online at https://doi.org/10.1016/j.heliyon.2024.e33601.

References

[1] J. Gollmer, A. Zirlik, H. Bugger, Mitochondrial mechanisms in diabetic cardiomyopathy, Diabetes Metab. J 44 (2020) 33–53, https://doi.org/10.4093/dmj.2019.0185.

[2] Y. Wu, T. Huang, X. Li, W. Cai, Retinol dehydrogenase 10 reduction mediated retinol metabolism disorder promotes diabetic cardiomyopathy in male mice, Nat. Commun. 14 (2023), https://doi.org/10.1038/s41467-023-36837-x.

[3] M. Hao, X. Huang, X. Liu, D. Yan, Novel model predicts diastolic cardiac dysfunction in type 2 diabetes, Ann. Med. 55 (2023) 766–777, https://doi.org/10.1080/07853890.2023.2180154.

[4] M. Wang, Y. Li, S. Li, J. Lv, Endothelial dysfunction and diabetic cardiomyopathy, Front. Endocrinol. 13 (2022) 851941, https://doi.org/10.3389/fendo.2022.851941.

[5] MJ de Blasio, N. Huynh, M. Deo, R.H. Ritchie, Defining the progression of diabetic cardiomyopathy in a mouse model of type 1 diabetes, Front. Physiol. 11 (2020) 124, https://doi.org/10.3389/fphys.2020.00124.

[6] G. Jia, V.G. DeMarco, J.R. Sowers, Insulin resistance and hyperinsulinaemia in diabetic cardiomyopathy, Nat. Rev. Endocrinol. 12 (2016) 144–153, https://doi.org/10.1038/nrendo.2015.216.

[7] M.H. Abukhalil, O.Y. Althunibat, S.H. Aladaileh, A.M. Mahmoud, Galangin attenuates diabetic cardiomyopathy through modulating oxidative stress, inflammation and apoptosis in rats, Biomed. Pharmacother. 138 (2021) 111410, https://doi.org/10.1016/j.biopha.2021.111410.

[8] Chen, D,Ruan, X,Liu, Y.He, Y,HMGCS2 silencing attenuates high glucose-induced in vitro diabetic cardiomyopathy by increasing cell viability, and inhibiting apoptosis, inflammation, and oxidative stress. Bioengineered; 13:11417–11429. https://doi.org/10.1080/21655979.2022.2063222.

[9] B. Jin, Y. Chen, J. Wang, Y. Wang, Costunolide alleviates hyperglycaemia-induced diabetic cardiomyopathy via inhibiting inflammatory responses and oxidative stress, J. Cell Mol. Med. 27 (2023) 831–845, https://doi.org/10.1111/jcmm.17686.

[10] J. Ren, J. Lin, L.Yan Yu, M,Lysophosphatidylcholine: potential target for the treatment of chronic pain, Int. J. Mol. Sci. 23 (2022), https://doi.org/10.3390/ijms23158274.

[11] Y. Zeng, A. Mtintsilana, J.H. Goedecke, E. Chorell, Alterations in the metabolism of phospholipids, bile acids and branched-chain amino acids predicts development of type 2 diabetes in black South African women: a prospective cohort study, Metabolism 95 (2019) 57–64, https://doi.org/10.1016/j.metabol.2019.04.001.

[12] X.-D. Zhao, F.-X. Wang, W.-F. Cao, Y. Li, TLR4 signaling mediates AP-1 activation in an MPTP-induced mouse model of Parkinson's disease, Int. Immunopharm. 32 (2016) 96–102, https://doi.org/10.1016/j.intimp.2016.01.010.

[13] Z. Yi, Y. Li, W. Ma, X. Wu, A novel KRAB zinc-finger protein, ZNF480, expresses in human heart and activates transcriptional activities of AP-1 and SRE, Biochem. Biophys. Res. Commun. 320 (2004) 409–415, https://doi.org/10.1016/j.bbrc.2004.05.182.

[14] A.A. Mukherjee, A.D. Kandhare, S.L. Bodhankar, Elucidation of protective efficacy of Pentahydroxy flavone isolated from Madhuca indica against arsenite-induced cardiomyopathy: role of Nrf-2, PPAR-γ, c-fos and c-jun, Environ. Toxicol. Pharmacol. 56 (2017) 172–185, https://doi.org/10.1016/j.etap.2017.08.027.

[15] E. Shaulian, M. Karin, AP-1 in cell proliferation and survival, Oncogene 20 (2001) 2390–2400, https://doi.org/10.1038/sj.onc.1204383.

[16] J.K. Nicholson, E. Holmes, J. Kinross, S. Pettersson, Host-gut microbiota metabolic interactions, Science. 336 (2012) 1262–1267, https://doi.org/10.1126/science.1223813.

[17] C.H. Liu, J. Ren, P.K. Liu, Amphetamine manipulates monoamine oxidase-A level and behavior using theranostic aptamers of transcription factors AP-1/NF-kB, J. Biomed. Sci. 23 (2016) 21, https://doi.org/10.1186/s12929-016-0239-2.

[18] A. Jadhav, S. Tiwari, P. Lee, J.F. Ndisang, The heme oxygenase system selectively enhances the anti-inflammatory macrophage-M2 phenotype, reduces pericardial adiposity, and ameliorated cardiac injury in diabetic cardiomyopathy in Zucker diabetic fatty rats, J. Pharmacol. Exp. Therapeut. 345 (2013) 239–249, https://doi.org/10.1124/jpet.112.200808.

[19] G.-D. Zhang, X.-X. Liu, J.-L. Liang, Q.-M. Hu, The distribution pattern of traditional Chinese medicine syndromes in 549 patients with type 2 diabetes, Diabetes Metab Syndr Obes 14 (2021) 2209–2216, https://doi.org/10.2147/DMSO.S295351.

[20] K. Gopal, Al Batran, R. Altamimi, T.R. Ussher JR., FoxO1 inhibition alleviates type 2 diabetes-related diastolic dysfunction by increasing myocardial pyruvate dehydrogenase activity, Cell Rep. 35 (2021) 108935, https://doi.org/10.1016/j.celrep.2021.108935.

[21] G. Jia, A. Whaley-Connell, J.R. Sowers, Diabetic cardiomyopathy: a hyperglycaemia- and insulin-resistance-induced heart disease, Diabetologia 61 (2018) 21–28, https://doi.org/10.1007/s00125-017-4390-4.

[22] N.M. Al-Rasheed, N.M. Al-Rasheed, I.H. Hasan, A.M. Mahmoud, Simvastatin ameliorates diabetic cardiomyopathy by attenuating oxidative stress and inflammation in rats, Oxid. Med. Cell. Longev. 2017 (2017) 1092015, https://doi.org/10.1155/2017/1092015.

[23] B. Lv, X. Yang, T. An, G. Jiang, Combined analysis of whole-exome sequencing and RNA sequencing in type 2 diabetes mellitus patients with thirst and fatigue, Diabetol. Metab. Syndrome 14 (2022) 111, https://doi.org/10.1186/s13098-022-00884-z.

[24] T.-Y. Wang, X.-Q. Zhang, A.-L. Chen, G.-J. Jiang, A comparative study of microbial community and functions of type 2 diabetes mellitus patients with obesity and healthy people, Appl. Microbiol. Biotechnol. 104 (2020) 7143–7153, https://doi.org/10.1007/s00253-020-10689-7.

[25] W. Yu, J. Huang, M. Lin, S. Wu, Fluorophore-dapagliflozin dyad for detecting diabetic liver/kidney damages via fluorescent imaging and treating diabetes via inhibiting SGLT2, Anal. Chem. 93 (2021) 4647–4656, https://doi.org/10.1021/acs.analchem.1c00223.

[26] P.K. Battiprolu, B. Hojayev, N. Jiang, J.A. Hill, Metabolic stress–induced activation of FoxO1 triggers diabetic cardiomyopathy in mice, J. Clin. Invest. 122 (2012) 1109–1118, https://doi.org/10.1172/JCI60329.

[27] N.G. Vallianou, T. Stratigou, S. Tsagarakis, Metformin and gut microbiota: their interactions and their impact on diabetes, Hormones (Basel) 18 (2019) 141–144, https://doi.org/10.1007/s42000-019-00093-w.

[28] K. Machiels, M. Joossens, J. Sabino, S. Vermeire, A decrease of the butyrate-producing species Roseburia hominis and Faecalibacterium prausnitzii defines dysbiosis in patients with ulcerative colitis, Gut 63 (2014) 1275–1283, https://doi.org/10.1136/gutjnl-2013-304833.

[29] L. Fizanne, A. Villard, N. Benabbou, R. Andriantsitohaina, Faeces-derived extracellular vesicles participate in the onset of barrier dysfunction leading to liver diseases, J. Extracell. Vesicles 12 (2023), https://doi.org/10.1002/jev2.12303.

[30] L. Zhang, J. Du, N. Yano, T.C. Zhao, Sodium butyrate protects -against high fat diet-induced cardiac dysfunction and metabolic disorders in type II diabetic mice, J. Cell. Biochem. 118 (2017) 2395–2408, https://doi.org/10.1002/jcb.25902.

[31] N. Zhao, Y. Ma, X. Liang, D. Bai, Efficacy and mechanism of qianshan huoxue gao in acute coronary syndrome via regulation of intestinal flora and metabolites, Drug Des. Dev. Ther. 17 (2023) 579–595, https://doi.org/10.2147/DDDT.S396649.

[32] Y. Yin, A. Sichler, J. Ecker, K.-P. Janssen, Gut microbiota promote liver regeneration through hepatic membrane phospholipid biosynthesis, J. Hepatol. 78 (2023) 820–835, https://doi.org/10.1016/j.jhep.2022.12.028.

[33] L. Zhang, C. Liu, Q. Jiang, Y. Yin, Butyrate in energy metabolism: there is still more to learn, Trends Endocrinol. Metabol. 32 (2021) 159–169, https://doi.org/10.1016/j.tem.2020.12.003.

[34] Z.-H. Zhao, Z.-X. Wang, Da Zhou, J.-G. Fan, Sodium butyrate supplementation inhibits hepatic steatosis by stimulating liver kinase B1 and insulin-induced gene, Cell Mol Gastroenterol Hepatol 12 (2021) 857–871, https://doi.org/10.1016/j.jcmgh.2021.05.006.

[35] A. Ossoli, S. Simonelli, C. Vitali, L. Calabresi, Role of LCAT in atherosclerosis, J. Atherosclerosis Thromb. 23 (2016) 119–127, https://doi.org/10.5551/jat.32854.

[36] K.J. Nass, E.H. van den Berg, E.G. Gruppen, R.P. Dullaart, Plasma lecithin:cholesterol acyltransferase and phospholipid transfer protein activity independently associate with nonalcoholic fatty liver disease, Eur. J. Clin. Invest. 48 (2018) e12988, https://doi.org/10.1111/eci.12988.

[37] S.I. Svetlov, E. Sturm, M.S. Olson, J.M. Crawford, Hepatic regulation of platelet-activating factor acetylhydrolase and lecithin:cholesterol acyltransferase biliary and plasma output in rats exposed to bacterial lipopolysaccharide, Hepatology 30 (1999) 128–136, https://doi.org/10.1002/hep.510300122.

[38] L. Zhou, A. Nilsson, Sources of eicosanoid precursor fatty acid pools in tissues, J. Lipid Res. 42 (2001) 1521–1542.

[39] S.-H. Lee, S.-Y. Park, C.S. Choi, Insulin resistance: from mechanisms to therapeutic strategies, Diabetes Metab. J 46 (2022) 15–37, https://doi.org/10.4093/dmj.2021.0280.

[40] J.-P. Huang, M.-L. Cheng, C.-H. Wang, L.-M. Hung, Therapeutic potential of cPLA2 inhibitor to counteract dilated-cardiomyopathy in cholesterol-treated H9C2 cardiomyocyte and MUNO rat, Pharmacol. Res. 160 (2020) 105201, https://doi.org/10.1016/j.phrs.2020.105201.

[41] T.N. Kim, M.S. Park, S.J. Yang, K.M. Choi, Body size phenotypes and low muscle mass: the Korean sarcopenic obesity study (KSOS), J. Clin. Endocrinol. Metab. 98 (2013) 811–817, https://doi.org/10.1210/jc.2012-3292.

[42] M. Yan, W.-B. Cai, T. Hua, X. Zhang, Lipidomics reveals the dynamics of lipid profile altered by omega-3 polyunsaturated fatty acid supplementation in healthy people, Clin. Exp. Pharmacol. Physiol. 47 (2020) 1134–1144, https://doi.org/10.1111/1440-1681.13285.
[43] P. Liu, W. Zhu, C. Chen, C. Peng, The mechanisms of lysophosphatidylcholine in the development of diseases, Life Sci. 247 (2020) 117443, https://doi.org/10.1016/j.lfs.2020.117443.
[44] X. Chen, J. Su, R. Wang, X. Wang, Structural optimization of cannabidiol as multifunctional cosmetic raw materials, Antioxidants 12 (2023), https://doi.org/10.3390/antiox12020314.
[45] R. Westbrook, T. Chung, J. Lovett, P.M. Abadir, Kynurenines link chronic inflammation to functional decline and physical frailty, JCI Insight 5 (2020), https://doi.org/10.1172/jci.insight.136091.